

Depth-Resolved Modulation of Metal–Oxygen Hybridization and Orbital Polarization across Correlated Oxide Interfaces

Paul C. Rogge, Padraic Shafer, Gilberto Fabbris, Wen Hu, Elke Arenholz, Evguenia Karapetrova, Mark P. M. Dean, Robert J. Green, and Steven J. May*

Interface-induced modifications of the electronic, magnetic, and lattice degrees of freedom drive an array of novel physical properties in oxide heterostructures. Here, large changes in metal–oxygen band hybridization, as measured in the oxygen ligand hole density, are induced as a result of interfacing two isovalent correlated oxides. Using resonant X-ray reflectivity, a superlattice of SrFeO₃ and CaFeO₃ is shown to exhibit an electronic character that spatially evolves from strongly O-like in SrFeO₃ to strongly Fe-like in CaFeO₃. This alternating degree of Fe electronic character is correlated with a modulation of an Fe 3*d* orbital polarization, giving rise to an orbital superstructure. At the SrFeO₃/CaFeO₃ interfaces, the ligand hole density and orbital polarization reconstruct in a single unit cell of CaFeO₃, demonstrating how the mismatch in these electronic parameters is accommodated at the interface. These results provide new insight into how the orbital character of electrons is altered by correlated oxide interfaces and lays out a broadly applicable approach for depth-resolving band hybridization.

orbital degrees of freedom and produce emergent electronic and magnetic properties in TMOs,^[1–4] a key question is what role do the underlying changes in metal–oxygen hybridization play? This uncertainty remains because while electronic and magnetic properties can be measured by existing techniques, metal–oxygen hybridization cannot be thus far probed in a quantitative manner across interfaces. Here, we deploy resonant soft X-ray reflectivity to depth resolve the oxygen ligand hole density arising from metal–oxygen hybridization and reveal that a superlattice consisting of two TMOs with similar electronic structures unexpectedly exhibits large changes in orbital character. By resolving the orbital character at the unit cell level, we find that the disparate orbital characters reconstruct at the interface, thus demonstrating a new class of oxide

The hybridization between transition metal *d* states and O *p* states is one of the defining features of transition metal oxides (TMOs) compared to conventional band insulators and metals, and the resulting mixed metal/oxygen character of the electronic structure plays a key role in their electronic properties. While it has been thoroughly demonstrated that formation of heterostructures can alter the charge, spin, and

interfacial reconstructions, that of metal–oxygen hybridization.

The important role of metal–oxygen hybridization is highlighted by the anomalous behavior of TMOs with strong metal–oxygen covalency. These materials have metal *d* and O *p* bands that directly overlap in energy—leading to a small or negative charge transfer energy—and gives rise to self-doped oxygen ligand holes due to the energetically favorable transfer

Dr. P. C. Rogge, Prof. S. J. May
Department of Materials Science and Engineering
Drexel University
3141 Chestnut St., Philadelphia, PA 19104, USA
E-mail: smay@drexel.edu

Dr. P. Shafer, Dr. E. Arenholz
Advanced Light Source
Lawrence Berkeley National Laboratory
1 Cyclotron Rd., Berkeley, CA 94720, USA

Dr. G. Fabbris, Dr. M. P. M. Dean
Department of Condensed Matter Physics and Materials Science
Brookhaven National Laboratory
98 Rochester St., Upton, NY 11973, USA


Dr. W. Hu
National Synchrotron Light Source II
Brookhaven National Laboratory
98 Rochester St., Upton, NY 11973, USA

Dr. E. Arenholz
Cornell High Energy Synchrotron Source
Cornell University
161 Wilson Laboratory, Synchrotron Drive, Ithaca, NY 14853, USA

Dr. E. Karapetrova
Advanced Photon Source
Argonne National Laboratory
9700 S Cass Ave, Lemont, IL 60439, USA

Prof. R. J. Green
Department of Physics and Engineering Physics
University of Saskatchewan
116 Science Pl, Saskatoon, Saskatchewan S7N 5E2, Canada

Prof. R. J. Green
Stewart Blusson Quantum Matter Institute
University of British Columbia
111-2355 E Mall, Vancouver, British Columbia V6T 1Z4, Canada

 The ORCID identification number(s) for the author(s) of this article can be found under <https://doi.org/10.1002/adma.201902364>.

DOI: 10.1002/adma.201902364

of electrons to the metal d states from the O $2p$ states ($d^n p^6 \rightarrow d^{n+1} p^5$).^[5–8] As a result, the electronic structure at the Fermi level can have dominant oxygen character, which has been used to explain many seemingly unexpected electronic and magnetic phenomenon such as superconductivity in the doped cuprates,^[9,10] incommensurate helical antiferromagnetism (SrFeO₃ and CaFeO₃),^[11–14] rapid suppression of antiferromagnetism due to doping (La_{2–x}Sr_xAO₄, A = Cu, Ni, Co),^[15,16] and the lack of Jahn–Teller distortions in formal e_g^1 perovskites (RNiO₃, R = rare earth element; SrFeO₃).^[5,17] Strong covalency can also alter the underlying mechanisms of metal–insulator transitions such that oxygen holes disproportionate on alternating metal sites rather than d electrons (RNiO₃, CaFeO₃).^[5,6,8,18,19] Moreover, strong hybridization can have a leading role in the magnetic order and conductivity of TMOs such as manganites as described in canonical work by Goodenough.^[20] Thus tuning metal–oxygen hybridization could bring about new electronic and magnetic properties in oxide heterostructures and enable new ways to achieve colossal property changes, for example, by tuning phase boundaries.

To measure changes in metal–oxygen hybridization at oxide interfaces, we synthesized a superlattice of the isovalent perovskite oxides CaFeO₃ and SrFeO₃ (formal Fe⁴⁺, d^4). These ferrate perovskites are strongly correlated materials that exhibit a metal–insulator transition and non-collinear magnetism with multi- q topological spin structures.^[11–14,21–23] Their negative charge transfer energy results in a large self-doped ligand hole contribution to their electronic structure^[11,12,17,24] such that the ground state is dominated by a configurational mixture of d^4 and $d^5 \bar{L}^1$,^[8] and the degree of ligand hole (\bar{L}^1) character is a measure of the Fe–O hybridization. While these ferrates have similar electronic structures, their crystal structures differ, where SrFeO₃ is cubic with 180° Fe–O–Fe bond angles and CaFeO₃ is orthorhombic with 158° bond angles.^[12] By measuring resonant reflectivity at spectroscopic signals that are sensitive to Fe–O hybridization, we find that the electronic character in confined CaFeO₃ layers is, unexpectedly, strongly Fe-like. This gives rise to a hybridization superstructure that spatially varies from strongly O-like in SrFeO₃ to strongly Fe-like in CaFeO₃. With the spatial resolution afforded by X-ray reflectivity, we find that these disparate electronic characters reconstruct within a single unit cell region at the interface. We support these findings by depth-resolving the Fe $3d$ orbital polarization using polarized resonant reflectivity, and show that the degree of orbital polarization correlates with the degree of Fe character, giving rise to an orbital superstructure through the superlattice and an orbital reconstruction at the interfaces. These results provide important insight into how oxide interfaces alter the orbital character of electrons. Additionally, our demonstration of resonant X-ray reflectivity for characterizing metal–oxygen interfacial reconstructions provides motivation and support for subsequent new ways to tune and identify the interfacial properties of complex oxide heterostructures.

The results in this study were obtained from a superlattice consisting of [(SrFeO₃)₂₀/(CaFeO₃)₅]₄ deposited on single crystal LaAlO₃(001) by oxygen-assisted molecular beam epitaxy. The off-resonance specular X-ray reflectivity measured at 800 eV, shown in **Figure 1a**, exhibits short-period oscillations associated with the total film thickness as well as superlattice

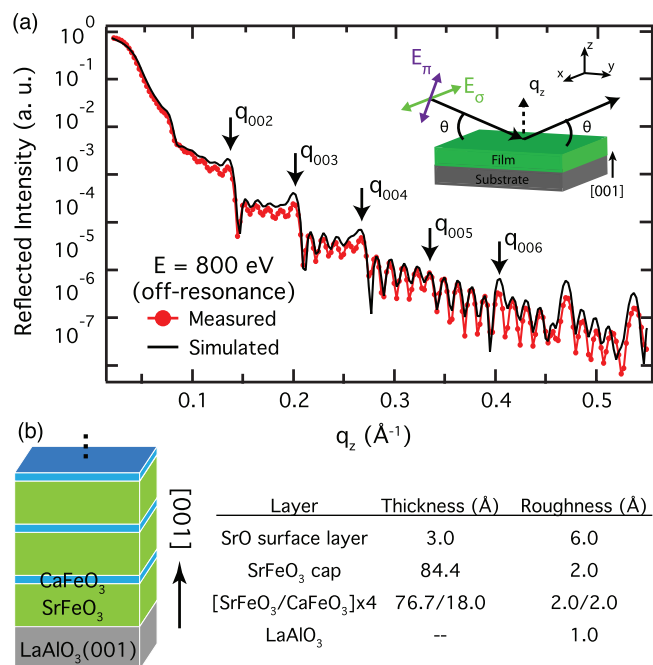


Figure 1. a) Measured (red) and simulated (black) off-resonant soft X-ray reflectivity at 800 eV for σ -polarized photons exhibits superlattice Bragg reflections q_{00L} . Inset illustrates the specular reflectivity measurement geometry. b) Schematic of the superlattice structure and the final film parameters obtained from the best reflectivity fit, which includes a 3 Å-thick SrO surface layer.

Bragg peaks, denoted by q_{00L} . The suppressed intensity of q_{005} is consistent with the 4:1 ratio of the SrFeO₃:CaFeO₃ thicknesses: For a superstructure of uniform subunits with thickness m and n , the structure factor of the $(m/n + 1)$ Bragg reflection is strongly suppressed.^[25,26] The film structure is further refined by fitting the measured data using the reflectivity analysis program ReMagX,^[27,28] and the final model parameters are listed in **Figure 1b**. The obtained interfacial roughness of 2.0 Å is less than the unit cell thickness, indicating abrupt interfaces. Hard X-ray diffraction shown in **Figure S1** in the Supporting Information further confirms the superlattice structure and suggests that the heterostructure is relaxed from the substrate, with the thinner CaFeO₃ layers instead strained to the thicker SrFeO₃ layers such that CaFeO₃ is under moderate tensile strain ($\approx 1.6\%$).

To probe Fe–O hybridization as a function of depth, we measured resonant reflectivity near the O K edge. The presence of oxygen ligand holes due to the strong Fe–O hybridization is spectroscopically observed as a pre-peak feature in the O K edge X-ray absorption (XA), and the pre-peak intensity is proportional to the ligand hole density.^[29–33] As seen in **Figure 2a**, the O K edge XA of separate, monolithic films of CaFeO₃ and SrFeO₃ exhibit a pre-peak at 526–529 eV. We note that both pre-peak intensities are suppressed compared to bulk when measured using this surface-sensitive total electron yield (TEY) technique and is attributed to partial oxygen loss at the film surface. Comparing the reflectivity at the oxygen pre-peak feature (528.5 eV) and at the nominal O K edge (530.1 eV, herein referred to as the O K edge), shown in **Figure 2b**, reveals two observations.

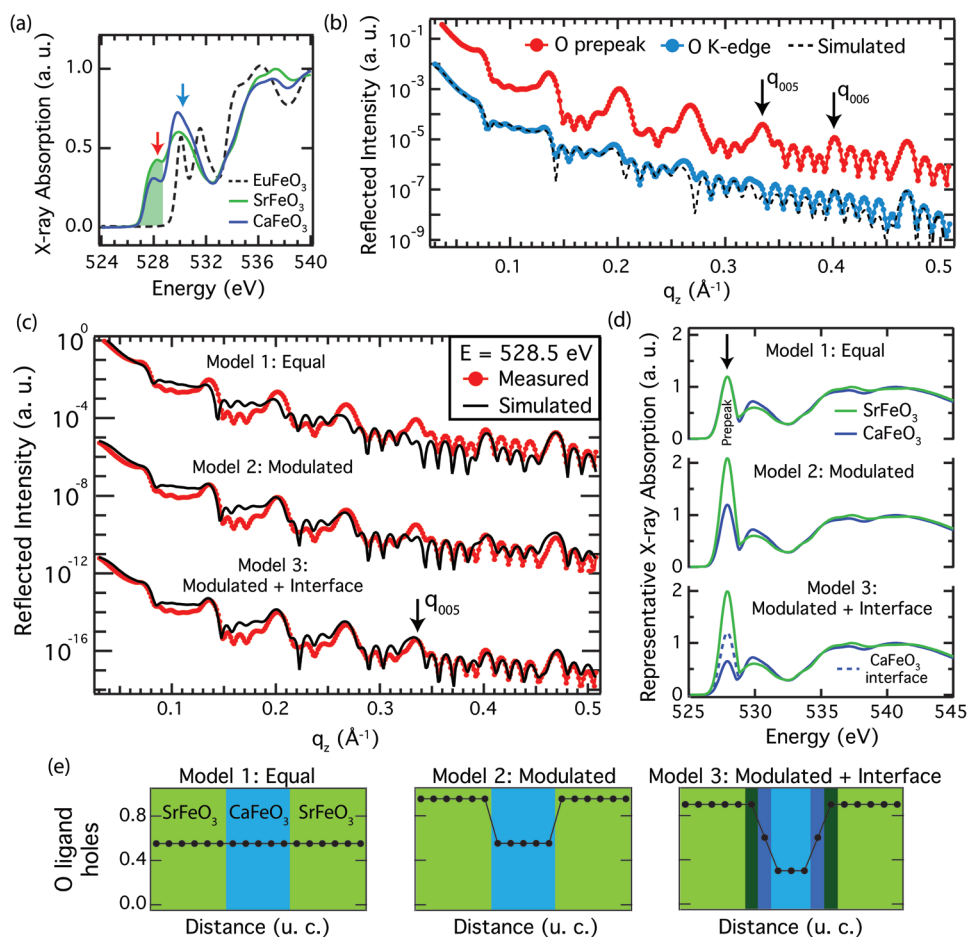


Figure 2. a) XA measured by TEY across the O K edge for monolithic films with Fe^{3+} (EuFeO_3 , dashed line) and formal Fe^{4+} (SrFeO_3 and CaFeO_3), which exhibit a pre-peak feature (526–529 eV, shaded) due to strong Fe–O hybridization in the ferrates. Arrows denote energies at which the resonant reflectivity was measured. b) Resonant reflectivity measured with σ -polarization at the O pre-peak (528.5 eV, red) and at the O K edge (530.1 eV, blue), along with the simulated reflectivity for the O K edge (530.1 eV, dashed, black line). c) Pre-peak reflectivity for three simulated scenarios. Model 1: an equal ligand hole density for SrFeO_3 and CaFeO_3 ; Model 2: different ligand hole densities for SrFeO_3 and CaFeO_3 ; and Model 3: a 1 unit-cell-thick region within each SrFeO_3 and CaFeO_3 layer at each interface is allowed to be distinct from the layer interior. d) The representative XA spectra with altered O pre-peak intensities that produced the best reflectivity fit for each model in (c) (arrow denotes the O pre-peak), where the SrFeO_3 pre-peak intensity is comparable to that measured in bulk SrFeO_3 .^[29] e) The estimated O ligand hole density (see the text) as a function of distance across the $\text{SrFeO}_3/\text{CaFeO}_3$ interfaces in the superlattice. Each data point (circle) represents one unit cell. Additional shades in Model 3 denote the interfacial regions.

First, the pre-peak reflectivity exhibits more intense superlattice reflections compared to the O K edge. Because the intensity of a Bragg reflection is proportional to the square of the difference of the energy-dependent scattering factors for the sublayers within the superlattice cell, which to first order corresponds to a difference in the effective electron density for SrFeO_3 and CaFeO_3 , this reveals that the CaFeO_3 and SrFeO_3 layers have a much larger difference in their O pre-peak scattering factors than their O K edge scattering factors, which we attribute to different ligand hole densities between the SrFeO_3 and CaFeO_3 layers. This is unexpected because previous work has estimated comparable ligand hole densities for SrFeO_3 (≈ 0.9 ligand holes)^[13,17] and CaFeO_3 (≈ 0.9 ligand holes).^[34] Thus, the sample exhibits a superstructure of modulated band hybridization.

Second, in contrast to the O K edge reflectivity, the pre-peak reflectivity exhibits enhanced intensity at the forbidden q_{005} reflection, which can occur if the scattering factors of the interface differ from the interior.^[25,26] This is strong evidence

for a reconstruction of the ligand hole density at the $\text{SrFeO}_3/\text{CaFeO}_3$ interface. To further support this analysis, the resonant reflectivity was simulated by computing the resonant complex refractive indices for SrFeO_3 and CaFeO_3 .^[35,36] Using the film structure determined previously in Figure 1, we simulate the reflectivity at the O K edge resonance energy (530.1 eV). As seen in Figure 2b, excellent agreement is achieved without the use of fitting parameters, where the superlattice reflections are well captured, including the suppressed q_{005} reflection at $q_z = 0.330 \text{ \AA}^{-1}$.

Next, we simulate three scenarios for the pre-peak reflectivity in Figure 2c. To model potential differences in ligand hole densities, we varied the O pre-peak XA intensity of both SrFeO_3 and CaFeO_3 and re-computed the resonant refractive index, $n = 1 - \delta + i\beta$ (see Methods and Figure S2, Supporting Information). The resulting relationship of δ and β at 528.5 eV (pre-peak energy) as a function of the modified pre-peak XA intensity was obtained and input into the reflectivity simulation software,

which enables the software to vary the pre-peak optical constants in order to determine the best fit. The pre-peak XA intensities for the SrFeO₃ and CaFeO₃ layers obtained from the best fit are plotted as the representative XA spectra in Figure 2d. The structural parameters determined in Figure 1 were maintained for all scenarios, and the numbers of free parameters are minimized by constraining the optical parameters to be equal for all SrFeO₃ layers and all CaFeO₃ layers.

Because bulk SrFeO₃ and bulk CaFeO₃ have similar ligand hole densities, in Model 1 we constrain the CaFeO₃ and SrFeO₃ layers to have an equal ligand hole density (i.e., one fitting parameter). Model 1 fails to replicate the enhanced intensity of the Bragg reflections, despite the large pre-peak intensity relative to the O K edge spectra associated with this fit, as illustrated in Figure 2d. We quantify the ligand hole density (discussed below) based on the pre-peak intensity obtained from the best fit and plot its spatial dependence through the superlattice in Figure 2e. For Model 2, we allow a modulated ligand hole density through the superlattice by allowing the SrFeO₃ and CaFeO₃ layers to have different ligand hole densities (i.e., two fitting parameters) and find that the best agreement occurs for a significantly enhanced SrFeO₃ ligand hole density compared to CaFeO₃. As seen in Figure 2c, the Bragg features of the measured reflectivity are now better captured, and the representative XA spectra shown in Figure 2d (Model 2) highlight the significantly increased pre-peak intensity of SrFeO₃ compared to CaFeO₃. However, the q_{005} reflection is not well captured by Model 2.

In Model 3, at each interface, we allow the ligand hole density of a 1 unit-cell-thick region within the SrFeO₃ and CaFeO₃ layers to be distinct from the ligand hole density of their respective layer interior (i.e., four fitting parameters). As seen in Figure 2c, the best fit is notably improved over Models 1 and 2, where the intensity of the forbidden q_{005} reflection is now replicated, and the agreement for $q_z > 0.3 \text{ \AA}^{-1}$ is additionally improved. We find that the best fit occurs when the SrFeO₃ interior and its 1 unit-cell-thick interfacial region have an equal ligand hole density, i.e., the ligand hole density is uniform through the entire SrFeO₃ layer. In contrast, the CaFeO₃ interior has a significantly lower ligand hole density than SrFeO₃ ($\approx 3\times$ less), and the 1 unit cell CaFeO₃ interfacial regions exhibit an average between these two extremes. This is illustrated in Figure 2d by the significant difference in pre-peak XA intensities obtained from the best fit in Model 3. Simulations of other interfacial reconstructions (e.g., 2 unit-cell-thick regions) produced poorer fits. Previous work has shown that reducing Fe–O hybridization via substitutional doping in La_(1-x)Sr_xFeO₃ results in a decreased O pre-peak intensity with no discernible shifts in the pre-peak position.^[29] These simulations therefore confirm a modulated electronic structure associated with Fe–O hybridization and reveal that the CaFeO₃ layers in this superlattice have a significantly lower ligand hole density than the SrFeO₃ layers, where the large pre-peak XA intensity obtained for SrFeO₃ in Model 3 is consistent with a bulk-like ligand hole density.^[29] The simulations indicate that the SrFeO₃ layers remain bulk-like whereas the ligand hole density of the much thinner, strained CaFeO₃ layers has been significantly reduced. Model 3 further demonstrates how the disparate electronic character is reconciled at the interface through a single unit cell

of CaFeO₃ that exhibits a degree of hybridization between that of the CaFeO₃ interior and SrFeO₃, as highlighted in Figure 2e (Model 3).

We gain further insights into band hybridization by measuring polarization-dependent reflectivity at the Fe *L* edge, which is sensitive not only to the Fe valence state but also the orbital occupation of the e_g electrons.^[36] The octahedral symmetry of perovskites splits the five 3*d* levels into a lower, triply degenerate manifold (t_{2g}) and a higher, doubly degenerate manifold (e_g). Further lowering of the local symmetry, for example, through epitaxial strain, can lift the degeneracy and split the two e_g orbitals, $d_{x^2-y^2}$ and $d_{3z^2-r^2}$, in energy such that the single e_g electron of the Fe *d*⁴ state preferentially occupies the lower energy orbital, whereas the filled e_g band of the d^5L^1 state would not result in different 3*d* orbital occupations. Given the hybridization superstructure, one would expect a commensurate superstructure of orbital character.

The polarization-dependent reflectivity measured at the Fe *L*₃ (708.9 and 709.4 eV) and *L*₂ edge (722.4 eV) (see Figure 3a, inset) is shown in Figure 3a. The data provide three initial insights. First, whereas the off-resonant (800 eV) and oxygen resonant reflectivity (528.5 and 530.1 eV) exhibit enhanced intensity at the Bragg reflections, in comparison the Bragg reflections of the Fe resonance energies at 708.9 and 709.4 eV have reduced intensity (see arrows in Figure 3a). This indicates that the structure factor, which depends on the difference in scattering factors between CaFeO₃ and SrFeO₃, is small and thus the resonant scattering factors for CaFeO₃ and SrFeO₃ are nearly equal at these energies. This is expected if both CaFeO₃ and SrFeO₃ have the same formal Fe⁴⁺ valence state because the optical parameters are derived from, and dominated by, the oxidation state-dependent XA spectra (see Figure S3, Supporting Information), although the Bragg intensity is not fully suppressed due to the different non-resonant contributions of Ca and Sr to the overall scattering factors. This supports the conclusion that the O ligand hole modulation is not due to oxygen vacancies, which would reduce the Fe valence and thus alter the Fe optical parameters.^[37] Second, rather than q_{005} , the q_{006} reflection exhibits behavior different from the other Bragg reflections. This mimics the O pre-peak reflectivity and suggests that the Fe states exhibit a similar reconstruction at the SrFeO₃/CaFeO₃ interface as the O ligand hole states. Third, the reflected intensity is polarization-dependent. The reflectivity measured with photons polarized perpendicular and parallel to the scattering plane, R_σ and R_π , respectively (see also Figure 1, inset), exhibit a phase shift, which we attribute to orbital polarization within the e_g band.

To extract the layer-resolved orbital polarization, we simulate the polarization-dependent reflectivity arising from different orbital polarizations^[36] within the SrFeO₃ and CaFeO₃ layers by using X-ray linear dichroism (XLD) spectra of monolithic SrFeO₃ and CaFeO₃ films measured previously (see Figure S3, Supporting Information).^[34] The simulated reflectivity of the final structure, shown in Figure 3b, exhibits good agreement with experiment. As seen in Figure 3c, the asymmetry of the measured reflected intensity, $(R_\sigma - R_\pi)/(R_\sigma + R_\pi)$, exhibits large features that, consistent with the superlattice structure, repeat in q_z . We determine the orbital polarization by fitting the asymmetry at 708.9 eV and then observe the resulting asymmetry at

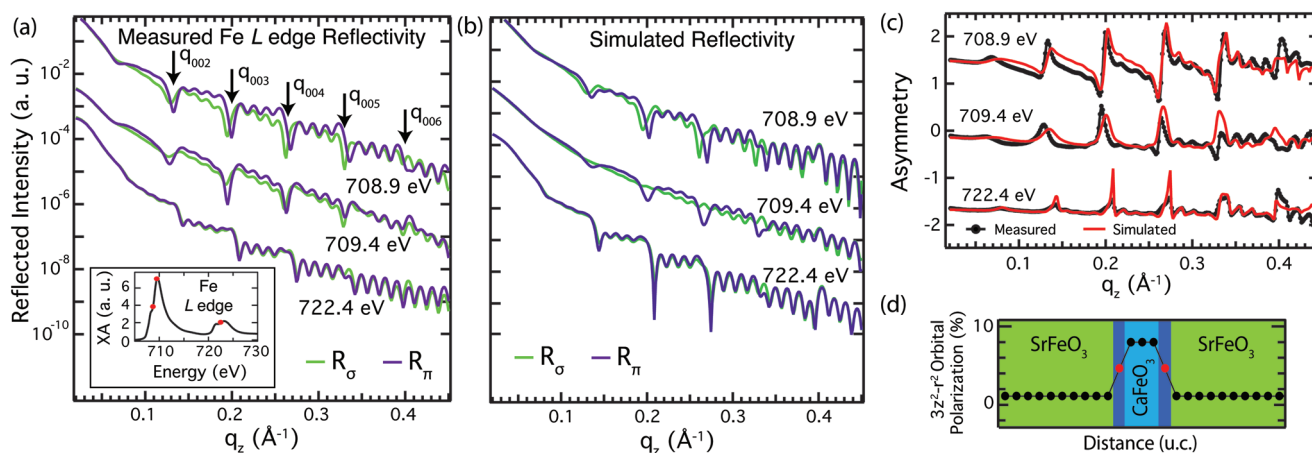


Figure 3. a) Resonant reflectivity at the Fe L edge measured with photons polarized perpendicular (R_σ) and parallel (R_π) to the scattering plane exhibits clear differences with photon polarization. Inset: Fe L edge XA for SrFeO₃; red circles denote reflectivity measurement energies. b) Simulated Fe resonance reflectivity replicates the polarization dependence after optimizing the orbital polarization within the layers. c) The reflectivity asymmetry, $(R_\sigma - R_\pi)/(R_\sigma + R_\pi)$, exhibits features that repeat in q_z in accordance with the film superstructure. The best fit with experiment is achieved when the SrFeO₃ layers have $\approx 1\%$ $d_{3z^2-r^2}$ polarization and the CaFeO₃ layers have $\approx 8\%$ $d_{3z^2-r^2}$ polarization that is reduced by approximately one-half within the 1 unit-cell-thick CaFeO₃ interfacial regions. d) Plot of the orbital polarization across the SrFeO₃/CaFeO₃ interfaces that produced the best fit with experiment.

the other two energies. Importantly, we enable the simulation software to vary the magnitude of the XLD (i.e., the magnitude of the orbital polarization) in order to determine the best fit with experiment (see Experimental Section). We first consider the structure with no interfacial regions and find that the best fit occurs for small $d_{3z^2-r^2}$ polarization in SrFeO₃ and much larger $d_{3z^2-r^2}$ polarization in the CaFeO₃ layers (see Figure S4, Supporting Information). A small orbital polarization in SrFeO₃ is consistent with its relaxed state and the strong $d^5\bar{L}^1$ contribution to its electronic character. The non-zero orbital polarization of the entire CaFeO₃ layer confirms that the effect is not simply a modification of the $d_{3z^2-r^2}$ orbitals due to the change in symmetry at the SrFeO₃/CaFeO₃ interface. The agreement between experiment and simulation notably improves when considering a distinct interfacial region. Based on the O pre-peak analysis, we consider a uniform SrFeO₃ layer and a CaFeO₃ layer with a 1 unit cell interfacial region at each interface. The best fit, shown in Figure 3c, identifies an electronic structure similar to the previous scenario albeit with a CaFeO₃ orbital polarization reduced by $\approx 40\%$ at its interface with SrFeO₃. This importantly highlights the interplay between Fe and O electronic character: The Fe⁴⁺ ground state is dominated by $(\alpha d^4 + \beta d^5\bar{L}^1 + \gamma d^6\bar{L}^2 + \dots)$ where $\alpha^2 + \beta^2 + \gamma^2 + \dots = 1$, and a reduction of the ligand hole density in the interior region of CaFeO₃ thus implies an increase in the d^4 contribution there. Because only d^4 contributes to the measured orbital polarization, the reduced Fe orbital polarization within the CaFeO₃ interface region is consistent with the increased ligand hole density there (see Model 3 in Figure 2e).

To quantitatively estimate the number of ligand holes, we normalize the representative SrFeO₃ pre-peak XA intensity obtained from the best reflectivity fit (Figure 2d, Model 3) to 0.9 ligand holes, which previous work has estimated for the ferrates.^[13,17,34] With this, the CaFeO₃ layers have ≈ 0.3 ligand holes in the interior and ≈ 0.6 ligand holes in the interfacial region, values that are significantly lower than previous estimates of

strained, monolithic films with ≈ 0.85 ligand holes,^[34] which further suggests that strain is not the source of the reduced ligand hole density. From a purely ionic view, these ligand hole counts imply that the number of Fe 3d electrons decreases from 4.9 in SrFeO₃ to 4.3 in CaFeO₃, values that we use in order to quantitatively estimate the measured orbital occupations using sum rules. Although the precise orbital polarization depends on the integral of the entire XLD spectrum, which we cannot fully determine here, the magnitude of the dichroism at these energies approximately scales linearly with strain,^[34] which we use to estimate the magnitude of the orbital polarization, $p = \frac{n_{3z^2-r^2} - n_{x^2-y^2}}{n_{3z^2-r^2} + n_{x^2-y^2}}$, where n_i is the number of electrons occupying orbital i . We find that SrFeO₃ has $\approx 1\%$ $d_{3z^2-r^2}$ polarization and CaFeO₃ has $\approx 8\%$ $d_{3z^2-r^2}$ polarization. The preferential $d_{3z^2-r^2}$ occupation under tensile strain for CaFeO₃ is consistent with previous measurements of monolithic CaFeO₃ films, where the inverted orbital polarization was shown to be consistent if strain effects were mostly limited to changes in Fe–O–Fe bond angles rather than bond lengths.^[34]

Such a substantial change in the Fe 3d occupation is unexpected given the approximately uniform charge density between SrFeO₃ and CaFeO₃. The significantly reduced Fe 3d occupation in the CaFeO₃ layers is interpreted as a change in the orbital character of the valence electrons in CaFeO₃, i.e., an increased d^4 contribution to the ground state at the expense of $d^5\bar{L}^1$ in the CaFeO₃ layers can account for the decreased Fe 3d occupation. This in turn implies that the valence electrons in the CaFeO₃ layers have an increased Fe orbital character at the expense of oxygen orbital character. Thus while bulk SrFeO₃ and bulk CaFeO₃ have valence electrons with strong oxygen character, this superlattice sample exhibits a significant modulation of orbital character along the growth direction, where the electronic structure varies from strongly oxygen-like in SrFeO₃ to strongly Fe-like in CaFeO₃. Moreover, our analysis demonstrates that these disparate orbital characters reconstruct within

a 1 unit-cell-thick region within CaFeO_3 at the $\text{SrFeO}_3/\text{CaFeO}_3$ interface.

Such a change in orbital character can be understood in terms of a change in the Fe–O hybridization, which depends on the energy separation between the Fe 3*d* and O 2*p* bands, Δ . The ligand hole density depends on the energy separation between the Fe and O bands and can be estimated using multiplet ligand field theory, which has successfully described strongly hybridized materials previously.^[8,38] We have calculated the relative contributions of d^4 , d^5L^1 , and d^6L^2 to the ground state as a function of Δ for CaFeO_3 (see Figure S5, Supporting Information). While $\Delta = -2.0$ eV for bulk CaFeO_3 with 0.85 ligand holes,^[17,34] we find that CaFeO_3 in superlattice form with 0.3 ligand holes corresponds to $\Delta = 6.0$ eV. Thus, this simple model indicates that the Fe–O hybridization in the CaFeO_3 layers is approximately equivalent to the situation where the Fe 3*d* states are significantly higher in energy than the O 2*p* states. This increased separation between the Fe and O states reduces the Fe–O hybridization and thus alters the orbital character of the valence electrons.

We ascribe the significant reduction in Fe–O hybridization within the CaFeO_3 layers to interface-induced changes to the local bonding environment. It is well known that epitaxial strain and symmetry mismatch at film/substrate interfaces alter B–O–B bond lengths and angles within ABO_3 perovskites, where the octahedral connectivity requirements at the interface can impart non-bulk rotations of the perovskite octahedra.^[39–42] Given that bulk SrFeO_3 has 180° bond angles and bulk CaFeO_3 has 158° angles, altered bond angles at the interface would be expected—particularly for the relatively thin, 5 unit-cell-thick CaFeO_3 layers sandwiched between thicker, 20 unit-cell-thick SrFeO_3 layers. Changes in bond angles are known to modify atomic hybridization by altering the overlap of the atomic orbitals,^[43–45] and the magnitude of the relative shift in the Fe 3*d*–O 2*p* energy alignment within the CaFeO_3 layers is consistent with previous work. First-principles calculations of CaFeO_3 estimate a change in the Fe 3*d*–O 2*p* energy alignment of ≈ 1 eV per degree change in the Fe–O–Fe bond angle,^[45] and bond angle changes on the order of 5° have been experimentally demonstrated in many perovskite systems due to imprinting.^[39–42,46,47] Techniques to measure bond angles are not possible here, however, because the 5 unit-cell-thick CaFeO_3 layers are too thin for half-order Bragg peak analysis and the superlattice is too thick for coherent Bragg rod analysis. Additionally, scanning transmission electron microscopy is not possible because these ferrates lose oxygen during sample preparation, which alters the Fe valence state and crystal structure. However, other strongly hybridized material systems that are not prone to oxygen loss, such as the rare-earth nickelates, could be studied to confirm our conclusions.

Based on our conjecture here, though, controlling interfacial and depth-dependent hybridization should be possible. Past work has demonstrated how epitaxial strain,^[39] ultra-thin films,^[40] superlattices^[46] and insertion of buffer layers^[47] can enable control over the B–O–B bond angles in perovskites. Thus, for example, increasing the CaFeO_3 layer thickness would be expected to localize hybridization changes to the interface alone as the CaFeO_3 bond angles relax towards their bulk values in the layer interior.^[39] Our demonstration using resonant X-ray

reflectivity to probe highly localized metal–oxygen hybridization is a critical step towards such a goal of controlling interfacial hybridization in oxide heterostructures.

In summary, we have experimentally shown that the formation of interfaces can significantly alter the degree of metal–oxygen hybridization in TMOs. Using resonant soft X-ray reflectivity at oxygen K edge energies sensitive to Fe–O hybridization, the electronic structure of a superlattice of SrFeO_3 and CaFeO_3 is found to modulate between strongly O-like in SrFeO_3 to strongly Fe-like in CaFeO_3 , reconciled within a single unit-cell-thick region at the interface. This spatially varying Fe character additionally gives rise to an artificial Fe 3*d* orbital superstructure. Previous discoveries of electronic, magnetic, and orbital reconstructions at oxide interfaces have enabled new strategies to tune functionality in these materials. Here, we demonstrate that metal–oxygen hybridization can be altered by and even reconstruct at oxide interfaces, and thus these results provide important context for understanding interfacial properties such as magnetism, superconductivity, and metal–insulator transitions which directly depend on ligand hole densities in metal oxides. We further propose that the resonant X-ray reflectivity approach as demonstrated here can be deployed broadly to probe new states of matter that are also sensitive to hybridization, such as topological insulators and semimetals.

Experimental Section

Material Synthesis: Ferrate superlattices were deposited by oxygen-assisted molecular beam epitaxy at $\approx 650^\circ\text{C}$ with a background oxygen pressure of 8×10^{-6} Torr (base pressure 4×10^{-10} Torr). The as-grown sample was subsequently annealed by heating to $\approx 600^\circ\text{C}$ in oxygen plasma (200 W, 1×10^{-5} Torr chamber pressure) and then slowly cooled to room temperature in oxygen plasma.^[24] Prior to all measurements, the films were re-annealed in oxygen plasma by the same post-growth process to mitigate oxygen deficiency. Immediately prior to deposition, elemental fluxes were confirmed to be approximately stoichiometric by depositing monolithic films of SrFeO_3 and CaFeO_3 that exhibited electrical transport consistent with stoichiometric films. Hard X-ray diffraction was performed at Sector 33-BM of the Advanced Photon Source.

Reflectivity Measurement and Analysis: Linearly polarized resonant X-ray reflectivity was performed at the Advanced Light Source (ALS), Beamline 4.0.2 and at the National Synchrotron Light Source-II (NSLS-II), Beamline 23-ID-1. Reflected intensity was measured at 300 K by a GaAsP diode and the diffuse scattering was accounted for by repeating the measurement with the sample offset by 1° and then subtracting these data (ALS) or was recorded by an area detector (fast CCD) with a $30\ \mu\text{m} \times 30\ \mu\text{m}$ pixel size such that the total intensity is the integrated intensity of a selected region-of-interest (NSLS-II). Reflectivity measured with π -polarized photons was normalized in order to account for the Brewster effect.^[36] The off-resonant and O K edge reflectivity were simulated using ReMagX in Paratt mode.^[27,28] The complex refractive index ($n = 1 - \delta + i\beta$) at the resonance energies was determined by combining experimentally measured XA across the O K edge and the Fe L edge for monolithic films of SrFeO_3 and CaFeO_3 on $\text{LaAlO}_3(001)$ with the non-resonant, tabulated data (Chantler tables^[48]) of the absorptive part of the scattering factor (f''). The dispersive part (f') was obtained by Kramers–Kronig conversion of f'' , and the refractive index (δ, β) was then obtained by conversion of f' and f'' .^[35,36] To model different ligand hole densities, the complex refractive index was calculated for different pre-peak XA intensities (see Figure S2, Supporting Information), and the values of δ and β at 528.5 eV (pre-peak energy) were then extracted from each modified spectrum for both SrFeO_3 and CaFeO_3 as a function of the pre-peak XA intensity. The resulting dependence of δ and β on the

pre-peak XA intensity was used to constrain the fitting optimization in ReMagX via the scripting capability for the 528.5 eV reflectivity.

The polarization-dependent Fe resonant reflectivity was simulated using a dielectric tensor that assumes a tetragonal distortion to the cubic (SrFeO₃) and pseudocubic (CaFeO₃) unit cells,

$$\epsilon = \begin{pmatrix} N_{xx}^2 & 0 & 0 \\ 0 & N_{xx}^2 & 0 \\ 0 & 0 & N_{zz}^2 \end{pmatrix} = \begin{pmatrix} \epsilon_{xx} & 0 & 0 \\ 0 & \epsilon_{xx} & 0 \\ 0 & 0 & \epsilon_{zz} \end{pmatrix}$$

where $N_{ij} = (1 - \delta_{ij} + i\beta_{ij})^{[36]}$ β_{xx} (β_{zz}) was derived from experimentally measured XA of monolithic films deposited on LaAlO₃(001) measured with photons polarized in-plane (out-of-plane) relative to the film surface. To model different orbital polarizations, the polarization-dependent difference between β_{xx} and β_{zz} , which is proportional to the XLD, was systematically modified by varying an XLD scaling factor, a :

$$\beta'_{xx} = \frac{\beta_{xx} + \beta_{zz}}{2} + a \left(\frac{\beta_{xx} - \beta_{zz}}{2} \right)$$

and

$$\beta'_{zz} = \frac{\beta_{xx} + \beta_{zz}}{2} - a \left(\frac{\beta_{xx} - \beta_{zz}}{2} \right)$$

Each β'_{xx} (β'_{zz}) spectrum was then converted to δ'_{xx} (δ'_{zz}) via Kramers–Kronig conversion. The values of δ'_{xx} , β'_{xx} , δ'_{zz} , and β'_{zz} at 708.9 eV were extracted as a function of the XLD scaling factor, a , which was used to constrain the fitting optimization for the 708.9 eV asymmetry. The XLD scaling factors for both SrFeO₃ and CaFeO₃ obtained from the best fit at 708.9 eV were used to generate the full-energy range of polarization-dependent optical parameters in order to simulate the reflectivity at the other Fe resonance energies.

Multiplet ligand field calculations were performed using the code *Quanty*.^[38] Calculation details are provided in the Supporting Information.

Supporting Information

Supporting Information is available from the Wiley Online Library or from the author.

Acknowledgements

P.C.R. and S.J.M. were supported by the Army Research Office, grant number W911NF-15-1-0133, and film synthesis at Drexel utilized deposition instrumentation acquired through an Army Research Office DURIP grant (W911NF-14-1-0493). R.J.G. was supported by the Natural Sciences and Engineering Research Council of Canada and M.P.M.D. was supported by the U.S. Department of Energy (DOE) Early Career Award Program under award number 1047478. This work used resources at the ALS, which is a DOE Office of Science User Facility under contract number DE-AC02-05CH11231, Beamline 23-ID-1 of the NSLS-II, a DOE Office of Science User Facility operated for the DOE Office of Science by Brookhaven National Laboratory under contract number DE-SC0012704, and Sector 33 of the Advanced Photon Source supported by the DOE Office of Science, Office of Basic Energy Sciences, under contract number DE-AC02-06CH11357.

Conflict of Interest

The authors declare no conflict of interest.

Keywords

band hybridization, oxide interfaces, resonant X-ray reflectivity, transition metal oxides

Received: April 12, 2019

Revised: August 22, 2019

Published online:

- [1] H. Y. Hwang, Y. Iwasa, M. Kawasaki, B. Keimer, N. Nagaosa, Y. Tokura, *Nat. Mater.* **2012**, *11*, 103.
- [2] P. Zubko, S. Gariglio, M. Gabay, P. Ghosez, J. M. Triscone, *Annu. Rev. Condens. Matter Phys.* **2011**, *2*, 141.
- [3] J. M. Rondinelli, N. A. Spaldin, *Adv. Mater.* **2011**, *23*, 3363.
- [4] Z. Huang, Ariando, X. R. Wang, A. Rusydi, J. Chen, H. Yang, T. Venkatesan, *Adv. Mater.* **2018**, *30*, 1802439.
- [5] T. Mizokawa, D. I. Khomskii, G. A. Sawatzky, *Phys. Rev. B* **2000**, *61*, 11263.
- [6] J. Matsuno, T. Mizokawa, A. Fujimori, Y. Takeda, S. Kawasaki, M. Takano, *Phys. Rev. B* **2002**, *66*, 193103.
- [7] G. A. Sawatzky, R. J. Green, in *Quantum Materials: Experiment and Theory*, Vol. 6 (Eds: E. Pavarini, E. Koch, J. van den Brink, G. Sawatzky), Forschungszentrum Jülich GmbH, Jülich, Germany **2016**, Ch. 1.
- [8] R. J. Green, M. W. Haverkort, G. A. Sawatzky, *Phys. Rev. B* **2016**, *94*, 195127.
- [9] F. C. Zhang, T. M. Rice, *Phys. Rev. B* **1988**, *37*, 3759.
- [10] R. Comin, R. Sutarto, F. He, E. H. da Silva Neto, L. Chauviere, A. Fraño, R. Liang, W. N. Hardy, D. A. Bonn, Y. Yoshida, H. Eisaki, A. J. Achkar, D. G. Hawthorn, B. Keimer, G. A. Sawatzky, A. Damascelli, *Nat. Mater.* **2015**, *14*, 796.
- [11] S. Kawasaki, M. Takano, R. Kanno, T. Takeda, A. Fujimori, *J. Phys. Soc. Jpn.* **1998**, *67*, 1529.
- [12] P. M. Woodward, D. E. Cox, E. Moshopoulou, A. W. Sleight, S. Morimoto, *Phys. Rev. B* **2000**, *62*, 844.
- [13] M. Mostovoy, *Phys. Rev. Lett.* **2005**, *94*, 137205.
- [14] S. Ishiwata, M. Tokunaga, Y. Kaneko, D. Okuyama, Y. Tokunaga, S. Wakimoto, K. Kakurai, T. Arima, Y. Taguchi, Y. Tokura, *Phys. Rev. B* **2011**, *84*, 054427.
- [15] C. H. Chen, S.-W. Cheong, A. S. Cooper, *Phys. Rev. Lett.* **1993**, *71*, 2461.
- [16] M. Cwik, M. Benomar, T. Finger, Y. Sidis, D. Senff, M. Reuther, T. Lorenz, M. Braden, *Phys. Rev. Lett.* **2009**, *102*, 057201.
- [17] A. E. Bocquet, A. Fujimori, T. Mizokawa, T. Saitoh, H. Namatame, S. Suga, N. Kimizuka, Y. Takeda, M. Takano, *Phys. Rev. B* **1992**, *45*, 1561.
- [18] A. Cammarata, J. M. Rondinelli, *Phys. Rev. B* **2012**, *86*, 195144.
- [19] J. Varignon, M. N. Grisolia, J. Iñiguez, A. Barthélémy, M. Bibes, *npj Quantum Mater.* **2017**, *2*, 21.
- [20] J. B. Goodenough, *Phys. Rev.* **1955**, *100*, 564.
- [21] M. Reehuis, C. Ulrich, A. Maljuk, C. Niedermayer, B. Ouladdiaf, A. Hoser, T. Hofmann, B. Keimer, *Phys. Rev. B* **2012**, *85*, 184109.
- [22] S. Chakraverty, T. Matsuda, H. Wadati, J. Okamoto, Y. Yamasaki, H. Nakao, Y. Murakami, S. Ishiwata, M. Kawasaki, Y. Taguchi, Y. Tokura, H. Y. Hwang, *Phys. Rev. B* **2013**, *88*, 220405.
- [23] S. Ishiwata, T. Nakajima, J. H. Kim, D. S. Inosov, N. Kanazawa, J. S. White, J. L. Gavilano, R. Georgii, K. Seemann, G. Brandl, P. Manuel, D. D. Khalyavin, S. Seki, Y. Tokunaga, M. Kinoshita, Y. W. Long, Y. Kaneko, Y. Taguchi, T. Arima, B. Keimer, Y. Tokura, **2018**, arXiv: 1806.02309v1 [cond-mat.str-el].
- [24] P. C. Rogge, R. U. Chandrasena, A. Cammarata, R. J. Green, P. Shafer, B. M. Leffler, A. Huon, A. Arab, E. Arenholz, H. N. Lee,

- T. L. Lee, S. Nemšák, J. M. Rondinelli, A. X. Gray, S. J. May, *Phys. Rev. Mater.* **2018**, 2, 015002.
- [25] S. Smadici, P. Abbamonte, A. Bhattacharya, X. Zhai, B. Jiang, A. Rusydi, J. N. Eckstein, S. D. Bader, J. M. Zuo, *Phys. Rev. Lett.* **2007**, 99, 196404.
- [26] H. Wadati, D. G. Hawthorn, J. Geck, T. Higuchi, Y. Hikita, H. Y. Hwang, L. F. Kourkoutis, D. A. Muller, S.-W. Huang, D. J. Huang, H.-J. Lin, C. Schüssler-Langeheine, H.-H. Wu, E. Schierle, E. Weschke, N. J. C. Ingle, G. A. Sawatzky, *J. Appl. Phys.* **2009**, 106, 083705.
- [27] S. Macke, A. Radi, J. E. Hamann-Borrero, M. Bluschke, S. Brück, E. Goering, R. Sutarto, F. He, G. Cristiani, M. Wu, E. Benckiser, H. U. Habermeier, G. Logvenov, N. Gauquelin, G. A. Botton, A. P. Kajdos, S. Stemmer, G. A. Sawatzky, M. W. Haverkort, B. Keimer, V. Hinkov, *Adv. Mater.* **2014**, 26, 6554.
- [28] S. Macke, E. Goering, *J. Phys.: Condens. Matter* **2014**, 26, 363201.
- [29] M. Abbate, F. M. F. de Groot, J. C. Fuggle, A. Fujimori, O. Strebel, F. Lopez, M. Domke, G. Kaindl, G. A. Sawatzky, M. Takano, Y. Takeda, H. Eisaki, S. Uchida, *Phys. Rev. B* **1992**, 46, 4511.
- [30] C. T. Chen, L. H. Tjeng, J. Kwo, H. L. Kao, P. Rudolf, F. Sette, R. M. Fleming, *Phys. Rev. Lett.* **1992**, 68, 2543.
- [31] J. Suntivich, W. T. Hong, Y. L. Lee, J. M. Rondinelli, W. Yang, J. B. Goodenough, B. Dabrowski, J. W. Freeland, Y. Shao-Horn, *J. Phys. Chem. C* **2014**, 118, 1856.
- [32] E. Pellegrin, J. Zaanen, H.-J. Lin, G. Meigs, C. T. Chen, G. H. Ho, H. Eisaki, S. Uchida, *Phys. Rev. B* **1996**, 53, 10667.
- [33] P. Abbamonte, L. Venema, A. Rusydi, G. A. Sawatzky, G. Logvenov, I. Bozovic, *Science* **2002**, 297, 581.
- [34] P. C. Rogge, R. J. Green, P. Shafer, G. Fabbri, A. M. Barbour, B. M. Leffler, E. Arenholz, M. P. M. Dean, S. J. May, *Phys. Rev. B* **2018**, 98, 201115.
- [35] S. Brück, *Ph.D. Thesis*, University of Stuttgart, **2009**.
- [36] E. Benckiser, M. W. Haverkort, S. Brück, E. Goering, S. Macke, A. Frañó, X. Yang, O. K. Andersen, G. Cristiani, H. U. Habermeier, A. V. Boris, I. Zegkinoglou, P. Wochner, H. J. Kim, V. Hinkov, B. Keimer, *Nat. Mater.* **2011**, 10, 189.
- [37] V. R. Galakhov, E. Z. Kurmaev, K. Kuepper, M. Neumann, J. A. McLeod, A. Moewes, I. A. Leonidov, V. L. Kozhevnikov, *J. Phys. Chem. C* **2010**, 114, 5154.
- [38] M. W. Haverkort, M. Zwierzycki, O. K. Andersen, *Phys. Rev. B* **2012**, 85, 165113.
- [39] J. M. Rondinelli, S. J. May, J. W. Freeland, *MRS Bull.* **2012**, 37, 261.
- [40] A. Y. Borisevich, H. J. Chang, M. Huijben, M. P. Oxley, S. Okamoto, M. K. Niranjan, J. D. Burton, E. Y. Tsybal, Y. H. Chu, P. Yu, R. Ramesh, S. V. Kalinin, S. J. Pennycook, *Phys. Rev. Lett.* **2010**, 105, 087204.
- [41] R. Aso, D. Kan, Y. Shimakawa, H. Kurata, *Sci. Rep.* **2013**, 3, 2214.
- [42] Z. Liao, N. Gauquelin, R. J. Green, S. Macke, J. Gonnissen, S. Thomas, Z. Zhong, L. Li, L. Si, S. Van Aert, P. Hansmann, K. Held, J. Xia, J. Verbeeck, G. Van Tendeloo, G. A. Sawatzky, G. Koster, M. Huijben, G. Rijnders, *Adv. Funct. Mater.* **2017**, 27, 1606717.
- [43] P. Garcia-Fernandez, J. A. Aramburu, M. T. Barriuso, M. Moreno, *J. Phys. Chem. Lett.* **2010**, 1, 647.
- [44] J. He, A. Borisevich, S. V. Kalinin, S. J. Pennycook, S. T. Pantelides, *Phys. Rev. Lett.* **2010**, 105, 227203.
- [45] A. Cammarata, J. M. Rondinelli, *J. Chem. Phys.* **2014**, 141, 114704.
- [46] J. Y. Zhang, J. Hwang, S. Raghavan, S. Stemmer, *Phys. Rev. Lett.* **2013**, 110, 256401.
- [47] Z. Liao, M. Huijben, Z. Zhong, N. Gauquelin, S. Macke, R. J. Green, S. Van Aert, J. Verbeeck, G. Van Tendeloo, K. Held, G. A. Sawatzky, G. Koster, G. Rijnders, *Nat. Mater.* **2016**, 15, 425.
- [48] C. Chantler, K. Olsen, R. Dragoset, J. Chang, A. Kishore, S. Kotochigova, D. Zucker, *Detailed tabulation of atomic form factors, photoelectric absorption and scattering cross section, and mass attenuation coefficients for Z = 1–92 from E = 1–10 eV to E = 0.4–1.0 MeV*. Technical Report, National Institute of Standards, **1995**.